Article

Not peer-reviewed version

Light Sheet Microscopy and 3D Analysis of Human iPSC-derived Embryoid Bodies

Mohammed Yusuf * , Jahan Salma * , Safana Farooq , Alessia Candeo , Archana Bhartiya , Atiqa Sajid , Marta Szynkiewicz , Ian Robinson , Stan Botchway , El-Nasir Lalani

Posted Date: 13 January 2023

doi: 10.20944/preprints202301.0238.v1

Keywords: induced pluripotent stem cells; embryoid bodies; light-sheet microscopy; multicolor fluorescence in situ hybridization; chromosomes

Article

Light Sheet Microscopy and 3D Analysis of Human iPSC-Derived Embryoid Bodies

Yusuf M [1,2,*], Salma J [1,*], Farooq S [1], Candeo A [3,4], Bhartiya A [2,5], Sajid A [1], Szynkiewicz M [3], Robinson IK [2,6] and Botchway SW [3], Lalani EN [1]

[1] Centre for Regenerative Medicine and Stem Cell Research, Aga Khan University, Karachi, P.O. Box 3500, 74800, Pakistan
[2] London Centre for Nanotechnology, University College London, London WC1H 0AH, UK
[3] Central Laser Facility, Science and Technology Facilities Council, Research Complex at Harwell, Didcot, Oxon, OX11 0FA, UK
[4] Department of Physics, Politecnico di Milano, Piazza Leonardo da Vinci 32, Milano, Italy
[5] Department of Chemistry, University College, London, UK
[6] Brookhaven National Lab, Upton NY 11973, USA
* Correspondence: moyusufcyto@gmail.com (Y.M.); salma.jahan@aku.edu (S.J.)

Abstract: Embryoid bodies (EBs) are multicellular three-dimensional (3D) aggregates generated from induced pluripotent stem cells (iPSCs) in suspension and serve as useful biological sources for many downstream applications. Imaging of live EBs has been hampered mainly due to the inherent limitations of the imaging techniques applied to date. This study aimed to image human iPSC (hiPSC) derived EBs to obtain their 3D volume, determining size, morphology, and cell viability from day 7 to 14 using Light Sheet Fluorescence Microscopy (LSFM). Furthermore, chromosomal stability was assessed using Multicolor fluorescence *in situ* hybridization (M-FISH) from day 8 to 14. EB volume increased from day 7 to 13 which, decreased at day 14. From day 7 to 11, the EBs mainly appeared spherical and morphed into an ellipsoidal shape by day 13. All EBs showed varied external morphologies and larger cavities at day 14. The EB karyotype was diploid 46XY at day 8 and exhibited a low level of aneuploidy from day 10 to 14. This study shows that an increase in cell death affects the morphology and chromosomal stability in EBs derived from hiPSC. We demonstrate that the combination of LSFM and M-FISH helps characterize EBs that will assist future stem cell therapies.

Keywords: induced pluripotent stem cells; embryoid bodies; light-sheet microscopy; multicolor fluorescence *in situ* hybridization; chromosomes

Introduction

Induced pluripotent stem cells (iPSCs)

[1] serve as an important biological material for many applications that include drug screening [2] disease modelling [3] and recapitulating early developmental events [4]. Like embryonic stem cells (ESCs), iPSCs are thought to have an unlimited self-renewal capacity and can be differentiated into three germ layers (mesoderm, ectoderm and endoderm) [1,5]. Furthermore, iPSCs can be directed to form organ-specific 3D structures called organoids [6,7]. These organoids are generated under specific culture conditions after producing multicellular aggregates known as embryoid bodies (EBs) [8]. Several quality control checks as recommended by the National Institutes of Health (NIH) are undertaken whilst cells are in culture and differentiated into specific lineages[9–13]. When EBs are produced, their size and shape are the first parameters to evaluate in order to assess their quality [14–16]. Previously, various 2D imaging modalities, including light and electron microscopy (EM), have been applied for assessing EB morphology that showed a distinctive central cavity [17–20]. 3D imaging allows complex analysis of biological structures such as depth and volume, thereby overcoming limitations of 2D imaging. Both confocal and multiphoton 3D imaging systems have been applied to study the 3D structure of EBs [21,22]. However, the former is limited in its depth/penetration and whilst the latter may require excessive average laser power for deep (>500

 doi:10.20944/preprints202301.0238.v1

μm) depths. These limitations have been overcome by using the Light Sheet Fluorescence Microscopy (LSFM).

LSFM allows high-speed imaging, spatial and temporal resolution and minimal sample damage by the excitation light source [23]. In LSFM, a thin sheet of light excites the fluorescence of an entire 2D plane, which is then collected with an objective generally held orthogonally to the illumination axis and recorded with a camera [24,25]. Since the fluorescence from out-of-focus planes is not excited, this approach allows for optical sectioning with reduced photobleaching and phototoxicity, making this method suitable for imaging live samples over prolonged periods [26,27]. LSFM has already been used to study embryonic development [28–31] but has yet to be explored for the detailed 3D assessment of EBs derived from human iPSCs (hiPSCs).

Efficient and controlled growth of EBs *in vitro* requires regular assessment according to recommended guidelines by the NIH as mentioned above [12]. Chromosomal stability is considered an important hallmark when working with stem cells as long-term culturing of pluripotent stem cells (PSCs) can result in the accumulation of culture-driven mutations. These mutations can pose a serious threat if utilised therapeutically, potentially leading to tumor formation *in-vivo* [32]. Therefore, it is critical to assess and identify genomic changes by performing karyotypic analysis (during culturing using both conventional Giemsa (G)-banding and more advanced multicolor [33,34]. Chromosomal aneuploidies have been observed at many stages fluorescence *in situ* hybridisation (M-FISH) technology [35–37]. The most common aneuploidies observed are chromosomes 1, 12, 17, 20, and X for both embryonic stem cells (ESCs) and iPSCs [38–41]. Even though karyotypic assessments are routinely performed on newly established iPSC lines and during prolonged culture [12,33,42,43] the number of studies performed to date analyzing the chromosomal stability in hiPSC derived EBs has been limited [19]. This highlights the critical need to assess chromosomal stability of EBs at various time points in culture, specifically before and after generation of EBs from iPSCs.

The study described here addresses the following aims: i) to generate and image live 3D volume of EBs using LSFM, ii) to quantify the overall size and 3D morphology of EBs, iii) to examine cell viability, and iv) to evaluate chromosomal stability using M-FISH.

Material and Methods

iPSC Cell Culture and Generation of Embryoid Bodies

hiPSCs-OX2-28 (p7) was provided by the James Martin Stem Cell Facility (European Bank for induced pluripotent Stem Cells (EBiSC), Oxford, UK). iPSCs were prepared according to previously published protocols [44,45]. Cells were cultured in feeder-free conditions in six-well plates (Thermo Fisher Scientific, UK) coated with Matrigel (Thermo Fisher Scientific, UK). iPSCs were maintained in mTeSR1-E8 media (Stem Cell Technologies, Cambridge UK), with the media changed daily. When cells became 70-80% confluent, they were treated with Accutase Cell Dissociation Reagent (Thermo Fisher Scientific, UK), giving a single-cell suspension. These dissociated cells were then transferred to a 15 ml conical tube (Thermo Fisher Scientific, UK) and were left to settle for 10 minutes, followed by centrifugation at 300× *g* for 5 minutes. These cells were gently resuspended in 10 ml of mTESR1-E8 media (Stem Cell Technologies, Cambridge UK). Before the generation of EBs, an Aggrewell plate was prepared according to the manufacturer's instructions (Stem Cell Technologies, Cambridge UK). Ten thousand cells were seeded into the Aggrewell plate in order to generate optimal sized EBs that were maintained in mTESR1-E8 media (Stem Cell Technologies, Cambridge UK), then incubated at 37°C, 5% CO_2, 95% air incubator (New Brunswick™ Galaxy® 170 R CO2 incubator, WAK-Chemie, Germany) for three days. Half media changes were performed on each day. EBs were then transferred into non-treated ultra-low attachment 6-well-plates (Stem Cell Technologies, Cambridge UK) and maintained in mTESR1-E8 media for additional 14 days.

Live/Dead Viability Assay

After seven days in culture, the viability of cells was assessed in EBs using a Live/Dead assay kit (Thermo Fisher Scientific, UK) performed according to the manufacturer's protocol. Simply, 200 μl

 doi:10.20944/preprints202301.0238.v1

of Live (Green) solution (component A) was added to 800 µl of growth media to prepare a 1 ml total volume that was then vortexed (for a few seconds) to ensure thorough mixing. The reagents were combined by transferring 4 µl of the Dead (Red) solution [(component B); (Propidium Iodide: stock solution 1 mg/ml, giving a 4 µg/ml working concentration] to the 1 ml Live (green-fluorescent calcein) solution. The resulting solution was vortexed for a few seconds to ensure thorough mixing. EBs were collected using a pipette and transferred to a glass bottom dish. Thereafter EBs were washed before the assay to remove any traces of growth media with 1x Dulbecco's phosphate-buffered saline (D-PBS) PH 7.4; (Thermo Fisher Scientific, UK). A mixture of Live Green/Dead Red solution was added directly to the dish containing EBs and incubated for 30 minutes at room temperature. After incubation, the staining solution was removed and 1 ml fresh growth media was added, and samples were transferred to the LSFM.

Light Sheet Fluorescence Microscopy

EBs were transferred gently using a pipette into an agarose holder that was prepared using a 3D printed mould shaped as a comb, as described in [46]. These holders could accommodate a minimum of 5 samples submerged in media that could be imaged sequentially with LSFM. Three EBs were imaged for each time point and condition (day 7- day 14). The LSFM that was used is the Leica TCS SP8 DLS. A light sheet was created by focusing the laser light with a 2.5X/0.07NA objective and scanning it at 1400 Hz with galvanometric mirrors. In this way, a so-called digital light sheet 3.7 µm thick and with a Rayleigh length of 240 µm is generated between two mirrors fixed around the detection objective, where the agarose holder and the sample are positioned. Due to the density of the samples, artefacts like blurring and the formation of stripes behind absorbing elements can occur. To limit these issues, two alternating counter-propagating light sheets were used for the fluorescence excitation of each plane. The two images were then merged via software. The emitted fluorescence is captured with a 10×/0.3NA objective and appropriately filtered accordingly to the emission of interest. The samples were imaged using two different laser lines of the excitation source, a supercontinuum laser (NKT Photonics) emitting at 80 MHz, coupled with the most suitable bandpass filter for the excitation and detection of the two stainings in use. For calcein the 488 nm laser band and a band-pass filter centered at 520 nm (Leica Filter DLS BandPass 504-545)) were used, while for propidium iodide the 561 nm laser line was selected together with a band-pass filter centered at 600 nm (Leica Filter DLS BandPass 575-635)). Both imaging channels were acquired for each plane before moving to the following one, in order to have the best overlap between channels.

A field of view of 735 µm×735 µm was collected with a 2048 ×2048 pixel camera (Hamamatsu Flash 4 V2), giving a pixel size of 0.359 µm. The sample was then moved through the light sheet, and images were acquired serially at 3 µm, producing stacks of images used to generate 3D reconstructions of the samples. The laser power at the sample was <200 µW and distributed in the light sheet.

Immunocytochemistry

Cultured iPSCs at day 3 were fixed using 4% paraformaldehyde (Electron Microscopy Sciences) for 20 minutes at room temperature, then permeabilized with 0.5% Triton X-100 (Sigma, Dorset, UK) for 5 minutes and rinsed with PBS. Cells were incubated in 10 % normal goat serum (Sigma, Dorset, UK) to block nonspecific antibody binding for 1 hour at room temperature. Subsequently, cells were incubated overnight at 4 °C with primary antibodies, Sox-2 (mouse, 1:500; Santa Cruz, California, USA) and Nanog (Rabbit, 1:500; Cell Signaling Technology, USA). On the second day, cells were washed three times for 5 minutes each in PBS at room temperature and then incubated in specific secondary antibodies at appropriate dilution (1:500), Alexa Fluor 488 anti-mouse and Alexa Fluor 594 anti-rabbit IgG conjugates (Thermo Fisher Scientific, UK) for 1 hour at room temperature in the dark. Cells were washed and incubated for 15 minutes at room temperature in Hoechst 33258 (1:10,000) (Sigma, Dorset, UK) for nuclear staining, then visualization of images was done using the Leica SP8 confocal microscope.

 doi:10.20944/preprints202301.0238.v1

Chromosomes Preparation

Metaphase chromosomes were prepared according to previously published protocols [3,55,67]. Briefly, cells were treated with KaryoMax colcemid (0.1 μg/ml) (Gibco Life Technologies, UK) for 15 hours followed by buffered potassium chloride (KCL) (0.075 M) treatment (Genial Genetics, UK) at 37 °C for 20 minutes. Samples were then fixed in Carnoy's solution (3:1 methanol/acetic acid) and stored at 4 °C until further use. Slides were prepared by dropping a small volume of suspension onto glass microscope slides and allowed to air-dry overnight. Chromosomes were prepared from EBs after dissociation using Accutase (Thermo Fisher Scientific, UK) for 15 minutes at 37 °C. The KaryoMax colcemid concentration was increased (0.2 μg/ml) (Gibco Life Technologies, Paisley, UK). Chromosome analysis (DAPI Vectashield, UK) counting and M-FISH was performed on iPSC cultures on days 8, 10, 11 and 14. Days 8, 11 and 14 were passage 9 and day 10 was passage 10.

Fluorescence In-Situ Hybridization

Fluorescence *in-situ* hybridization (FISH) was performed according to the manufacturer's instructions (MetaSystems, Germany, http://www.metasystems-international.com) and a previously published protocol [47,48]. A 2-color FISH was done by mixing two directly labelled chromosome-specific probes, Xcyting Chromosome paint 9 (XCP9) in Orange and Chromosome paint 2 (XCP 2) in Green (MetaSystems, Germany). FISH was done using the hot block method (MetaSystems, Germany, http://www.metasystems-international.com). Slides were immersed into an ethanol series 75%, 85% and 100%. 10 μl of the probe was applied to the slide, covered with a 22 × 22 mm coverslip, and sealed using rubber cement. The slide was denatured at 75 °C for 3 minutes on a hot block and then left to hybridize overnight in an incubator at 37 °C. Washes were done using 0.4xSSC at 72 °C for 2 minutes followed by a wash with 2xSSC containing 0.05% Tween20 at room temperature for 30 seconds. All slides were mounted with DAPI (Vectashield, UK). Images were captured using a Z2 fluorescence microscope (Zeiss, UK) and analyzed using the ISIS software from MetaSystems (Zeiss, UK).

Multicolor Fluorescence In-Situ Hybridization

M-FISH was performed using a 24Xcyte mFISH probe kit (MetaSystems, Germany) according to manufacturer's (MetaSystems, Germany, http://www.metasystems-international.com) and previously published protocols [37,47–49]. Briefly, slides were washed in an ethanol series 70%, 85% and 100% ethanol for 1 minute each and then left to air dry. The sodium hydroxide (NaOH); (0.07 N) denaturation was performed on the slide that was then placed into ethanol (30%, 70%, 90%, and 100%) for dehydration and left to air dry. The M-FISH probe was denatured at 75°C for 5 minutes and re-annealed in incubation at 37°C for 30 minutes). 10 μl of the probe was applied and left at 37°C for at least 72 hrs. The unbound probe was removed by washing at 72 °C (+/− 1 °C) using 0.4 x SSC for 2 minutes. The slides were further incubated into a coplin jar containing 2 x SSC with Tween 20 for 30 seconds. A brief rinse was done using Milli-Q water at room temperature, and the slides were left to air dry. Images were captured using a Z2 Zeiss fluorescence microscope (Zeiss, UK) and analyzed using the ISIS software from MetaSystems (Zeiss, UK).

3D Modeling and Analysis of Embryoid Bodies

Raw Leica image files obtained with LSFM were analysed using AVIZO (Thermo Fisher Scientific, UK). Live and dead cells were segmented in an automated fashion based on different channels in the software. Quantitative analysis of individual EB diameter and volume (after performing live and dead assay) was done. Diameter measurements (μm) were taken for separate EBs using the "measure" tool (line) in the Avizo project view from the object (EBs) center. Volume measurements (nm^3) for individual EBs were taken from Avizo "Material statistics" module after using the "Threshold" tool in the Avizo selection panel.

 doi:10.20944/preprints202301.0238.v1

Results

Growth Characterization of EBs

Expression of SOX2 and NANOG was assessed in iPSCs (p9) following revival and during the generation of EBs (Figure S1A,B) and showed co-localisation indicating pluripotent expression (Huangfu et al, 2008). First we examined the size of EBs in *vitro* after performing measurements from reconstruction obtained after LSFM (Figure 1A-E). We observed an increase in the average diameter of EBs ranging from 184.2±5.03 µm at day 7 to 422.5±59.38 µm at day 13 (Figure 1 A-E and 1K; Figure S2A-E (i-ii) and F; Table S1). The average diameter of EBs decreased from 422.5±59.38 µm at day 13. to 395.3±63.79 µm at day 14 (Figure 1E and 1K; Figure S2E(i-ii); and Table S1**)** Diameter analysis of individual EBs at day 7 (EB1-181.77 µm, EB2-180.87 µm, EB3-190.01 µm), day 10 (EB1-276.6 µm, EB2-254.67 µm and EB3-279.98 µm), and day 11 (EB1-274.09 µm, EB2-269.65 µm and EB3-286.72 µm) showed similar diameters to one another (Figure S2F and Table S1). The highest variation in diameter was observed amongst EBs at day 13 (EB1-489.89 µm, EB2-399.76 µm and EB3-377.85 µm) and day 14 (EB1- 441.94 µm, EB2- 421.46 µm and EB3- 322.64 µm) (Figure 1K and Figure S2F). Thus, on average, day 13 EBs (Figure 1D and 1K; Figure S2D) exhibited the largest diameter in size compared to other EBs that were examined at days 7, 10, 11, and 14 (Figure 1K).

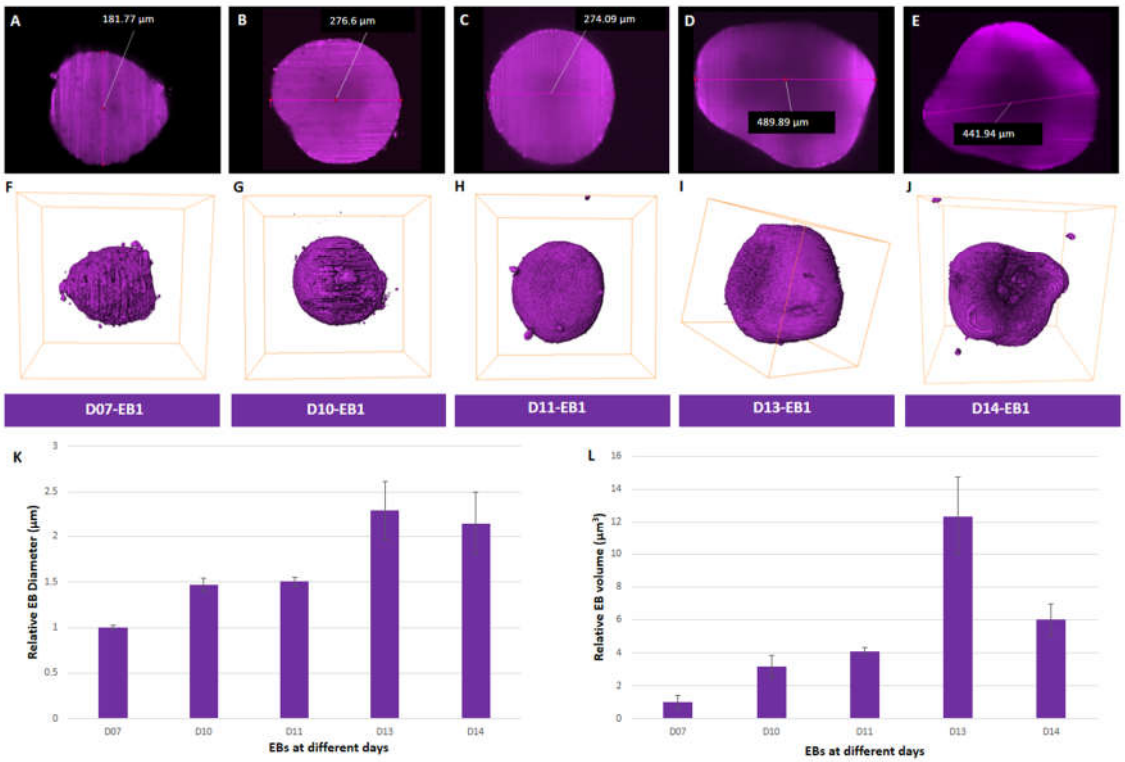

Figure 1. Growth characterization of EBs. (A-E) Diameter of EBs at day 7-14. (F-J) Volume rendering of EBs at day 7-14. (K) Relative diameter and (L) volume of EBs at different days. Bounding box size for each EB (F-J) is given in Supplementary Table 1.

We then evaluated the volume of segmented EBs (Figure 1F-J, Figure S2A-E (iii-iv), Table S1, Movies S1 and 2) in order to get a complete representation of their dimensionality. Average volumes of EBs from day 7 (0.0036±0.0015 mm^3) to day 11 (0.0147±0.0008 mm^3) showed a 4-fold increase (Figure 1L). EBs showed a 3-fold increase in volume from day 11 (0.0147±0.0008 mm^3) to day 13 (0.0442±0.0085 mm^3) (Figure 1L, Table S1). However, a 2-fold decrease in volume was observed in EBs (0.0442±0.0085 mm^3 to 0.0215±0.0034 mm^3) from day 13 to 14 (Figure 1L, Figure S2H, Table S1). Amongst all the EBs analyzed, the most variability in volume was seen at days 13 and 14 compared to days 7 to 11 (Figure 1L, Figure S2H; Table S1). Day 13 EB2 had the largest volume of all EBs

 doi:10.20944/preprints202301.0238.v1

analysed (Figure S2D(iii) and 2H, Table S1). In summary, we observed an increase in both average diameter and volume of EBs over the period of growth up to day 13, followed by a decrease at day 14.

3D Cell Viability Assessment of EBs

To examine cell viability in EBs, live/dead assay was performed at days 7, 10, 11, 13 and 14. EBs contained both viable and dead cells at all-time points (day 7 to 14), indicated by green and red staining, respectively (Figure 2A-E (i-iii) and F; Figure S3A-E (i-ii(a-c) and F, Table S1, Table S2). Live cells were predominantly present on the outer surface of EBs with some EBs showing dead cells attached to the outer surface of the EB and also scattered around the surrounding area (<0.14% of total dead percentage) (Table S1 and Table S2). Live and dead cells percentage in all EBs showed a notable difference from day 11 to day 14. The average percentage of dead cells remained below 1.7% from day 7 (0.5±0.17%) to day 11 (1.61±1.16%) (Figure S3F; Table S1). The average percentage of dead cells increased from day 11 (1.61±1.16%) to day 13 (20.3±4.99%) (Figure 2D,F; Figure S3D,F; Table S1. At day 13 EBs displayed a dense core packed with dead cells (Figure 2D,F; Figure S3D and 3F; Table S1; Table S2; Movie S3). At day 14, the average percentage of dead cells dropped to 2.53±0.46% (Figure 2E and 2F; Figure S3E and 3F; Table S1; Movie S4) from day 13 (20.3±4.99%). Overall, an increase in dead cell percentage from day 11 to day 13 was seen, followed by a decrease at day 14.

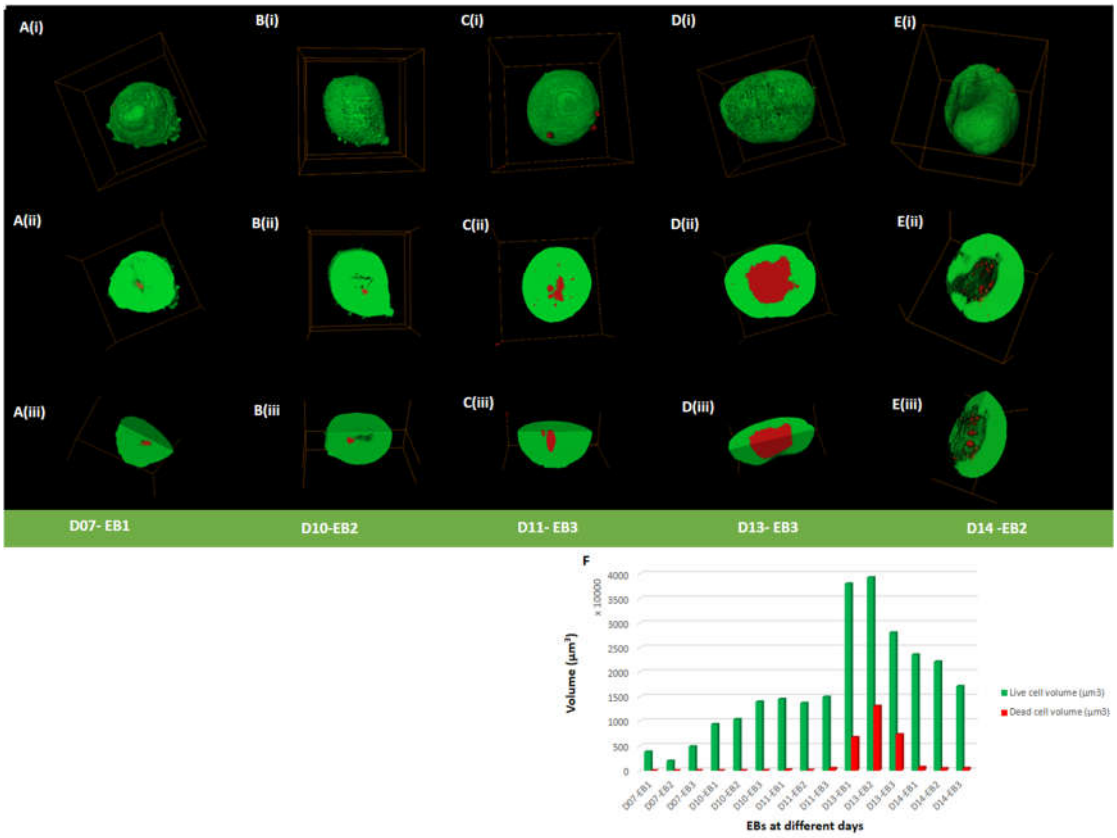

Figure 2. 3D Viability Assessment of EBs. (Ai-Ei) Volume rendering of EBs at day 7-14. (Aii-Eii) Cross-sections taken from the middle of the EBs (Aiii-Eiii) Further cross-sectional view of (Aii-Eii). (F) Graph shows the volume of live and dead cells of different EBs at the different days. Green shows live and red shows dead cells. Bounding box size for each EB is given in Supplementary Table S1.

 doi:10.20944/preprints202301.0238.v1

3D Morphological Analysis of EBs

Morphological analysis of EBs was carried out from day 7 to day 14 and is summarized in Table S3. Day 7 to day 11 EBs appeared to have spherical shapes (Figure 3A-C; Figure S4A-C), except day 7 EB2 (Figure 3A) and day 11 EB2 (Figure 3C) that had ellipsoidal shapes. Ellipsoidal shapes were seen in all day 13 EBs (Figure 3D; Figure S4D). In comparison, all three EBs at day 14 showed varied morphologies, EB1 being irregular shaped (Figure S4E (ii-iv)), EB2 being ellipsoidal (Figure S4E (i-iii)), and EB3 being spherical (Figure 3E).

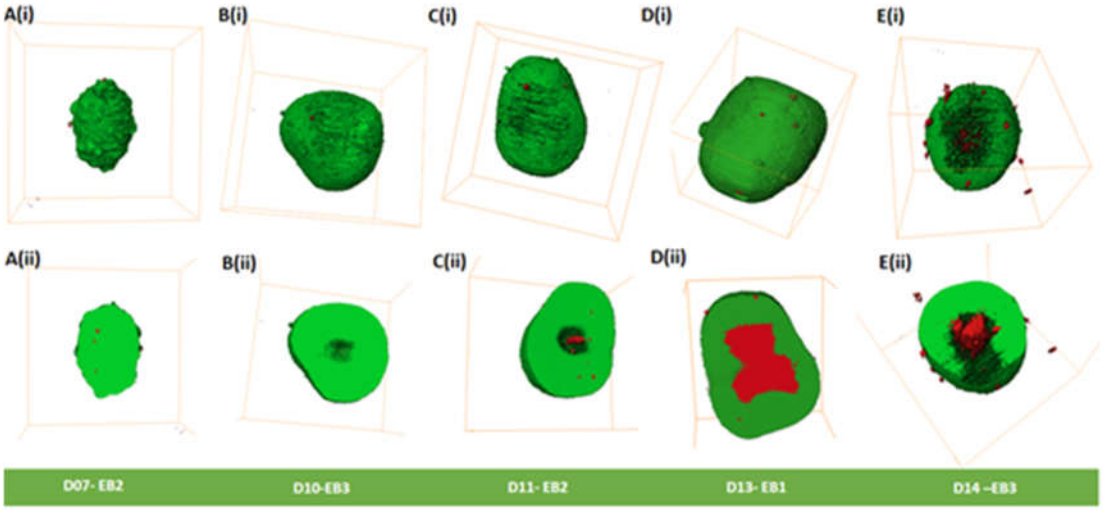

Figure 3. 3D morphological analysis of EBs. (Ai-Ei) Volume rendering of EBs from day 7-14. (Aii-Eii) Cross-sections taken form the middle of the EBs from Ai-Ei. Green shows live and red shows dead cells. Bounding box size for each EB is given in Supplementary Table 1.

Cavities (spaces) were observed on the outer surface of EBs mainly from days 13 and 14 (Figure 3D (i) and E (i); Figure S4D and E; Table S3). We observed in day 14 EBs outer cavities that extend from the inner core of the EBs to the periphery with dead cells on the outer surface(Figure 3E); Figure S4E, Movie S4, Table S3). We did not observe cavitation along the external margin of the EBs between days 7-11. However, we did observe dead cells (Figure 3A (i)-C(i); Figure S4 A-C; Table S3). Dead cells were observed on the outer surface of all EBs (day7 – 14); (Figure 3A(i)-E(i), Figure S4A-E; Table S2) that contribute to less than 0.15% of the dead cells Table S1). Dead cells were observed inside all EBs (day7 -14), with some showing cavities (Table S3).

Karyotypic Analysis

We examined the chromosomal stability of EBs at days 8, 10, 11, and 14. Chromosomal stability of EBs was assessed using M-FISH and DAPI counting; results are summarized in Table S4 and 5. Chromosome prepared from EBs displayed typical chromosome morphologies to the revived iPSC line (2D); (Figure 4Ai and 4Aii).

 doi:10.20944/preprints202301.0238.v1

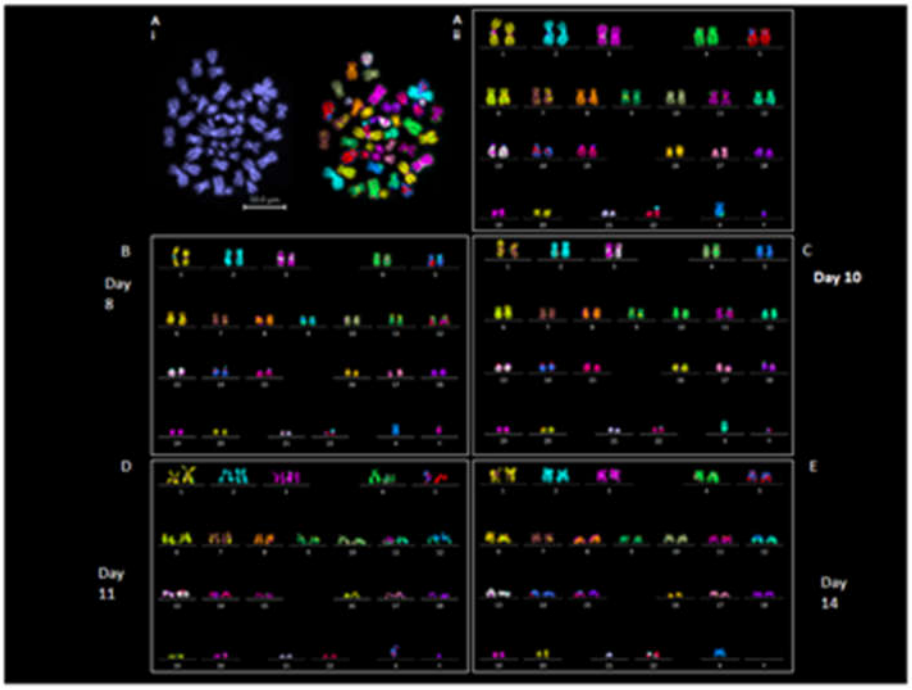

Figure 4. Karyotypic analysis of revived iPSCs and derived EBs. (Ai) DAPI and M-FISH spreads of 2D iPSC cells. (Aii) Karyotype of M-FISH spread in Ai showing 46XY. M-FISH karyotypes from EBs at (B) Day 8 (46XY), (C) day 10 (46XY), (D) day 11 (46XY) and (E) Day 14 (43X, -21,-Y).

The iPSC was diploid (46XY), metaphase spreads prepared from EBs (3D) derived from iPSCs on day 8 (n = 15) and day 10 (n =8) exhibited normal 46XY karyotypes in all the cells analyzed (Figure 4B-C) except 1 cell from day 10 that showed 45XY (missing chromosome 9) (Table S4). Chromosome spreads analyzed from day 11 (n = 8) and day 14 (n = 13) EBs were also 46 XY except for 2 spreads from day 11 and 4 spreads from day 14 that showed aneuploidy (Figure 4D-E; Table S4). DAPI counting was performed on 30 chromosome spread from both 2D iPSCs and derived 3D EBs at each day (Table S5). Spreads prepared from day 8 to day 10 EBs showed 46XY in all cells analyzed. Aneuploidy was observed in 5 out of 30 cells from day 11 and day 14 EBs, (Table S5). A suspected insertion of chromosome 2 material on chromosome 22 was observed in some M-FISH karyotypes. This was validated by applying FISH using a whole chromosome probe hybridization for chromosomes 2 and 22. No actual insertion of chromosome 2 on chromosome 22 was found (Figure S5).

Discussion

The study described here addresses the following aims: i) to generate and image live 3D volume of EBs using LSFM, ii) to determine the overall size and 3D morphology of EBs, iii) to examine cell viability, and iv) to evaluate chromosomal stability using M-FISH.

EBs derived from iPSCs are essential for developing differentiated cell types for study and potential therapeutic application. The current work was done to understand the 3D growth of hiPSC-derived EBs that remains understudied to date. LSFM has been demonstrated as a useful imaging approach that is transforming our understanding of live mammalian developmental processes [50]. Furthermore, LSFM has been used for studying cortical organoid development using hiPSC [51] and their derived EBs differentiated into the cerebral organoids [6]. To our knowledge, this is the first study that utilizes LSFM to evaluate individual hiPSC derived EBs over a 14-day period. LSFM has shown advantages compared to standard optical sectioning techniques like confocal microscopy, the main one being the capability to reach in depth tissue, even is EBs with diameters larger than 400 μm.

 doi:10.20944/preprints202301.0238.v1

This is possible thanks to the 90° configuration typical of LSFM. Besides, the technique allows one to mount samples in holders that maintain the native EBs 3D configuration, without pressing them onto microscopy slides. This becomes important when trying to quantify the volume of the EBs.

We determined changes in iPSC derived EB's morphology, size, volume and cell viability. Simultaneously we also assessed the karyotypic stability of EBs using M-FISH technology. Most data cited in the literature assesses the size of EBs using diameter measurements [2,47,50]. This study undertook volumetric assessment after imaging individual hiPSC derived EBs using LSFM. The hiPSC derived EBs increased in volume from day 7 to 13, which reduced at day 14. Son et al, 2011 reported a decrease in diameter similar to our study around day 14, suggesting this may be a stage-specific feature of EBs. In this study, EBs derived from hiPSC had diameters ranging from 180 μm (smallest) to 422 μm (largest). Studies undertaken using mouse ESCs (mSECs) derived EBs are between 100 μm to 500 μm [14,52]. Such studies examining the diameter and morphology have suggested that the change is important for lineage-specific differentiation [15,16,53].

hiPSC derived EBs assessed in our study have a spherical shape up to day 11 thereafter, they become heterogeneous predominantly ellipsoidal and irregular shaped by day 14. A similar morphological pattern has been observed in EBs derived from mESCs where spherical shapes were seen in the first 2 days of culture that then become ellipsoidal by day 3 and elongated by day 4 [54]. Even though similar morphologies were seen between mouse and human derived EBs, the timing of development *in vitro* is varied. Spherical morphology has also been found in previous studies that assessed EBs derived from hESCs and hiPSC at day 7 [19,55]. Neither of these studies applied 3D LSFM. Our study provides the first detailed analysis of hiPSC derived EB for developmental characteristics *in vitro*.

We found dead cells in all our observed EBs some with and others without cavities. Internal cavities started from day 7 and were present in all day 14 EBs. We also observed a structural change in day 13 EBs, whereby outer cavities began to appear. In comparison, day 14 EBs displayed extended cavities that merged into the central core of the EBs. These cavities have been documented previously as cystic EBs and are commonly seen in hESC derived Ebs [11,17,56,57] and in hiPSC derived EBs [19]. These EBs are known to recapitulate early embryonic developmental events [58]. During the development of mESC derived EBs, a dense core region containing dead cells have been observed at earlier stages of development, indicating their importance in organism development [59–61]. In our study, smaller EBs (seen in day 7 to day 11) displayed a lower percentage of dead cells in the core as compared to day 13 that showed a large dense region containing dead cells. It has been shown previously that larger EBs contain a necrotic core [62–64]. This occurs due to poor diffusion of nutrients and oxygen in the center of the clusters [64]. This affects the viability, proliferation and differentiation of cells *in vivo* and *in vitro* [65,66] and is most likely the case in our observed EBs.

Assessing the genomic stability of iPSCs is vital as alterations are known to occur during *in vitro* propagation. Majority of the studies done to date have focused on investigating chromosomes from 2D iPSC cultures [35,37,40,41]. This is essential for their use in disease modeling and downstream therapeutic applications [67]. In this study, we screened chromosomes from iPSC derived EBs as this has been understudied. Normal (46 XY) karyotypes were observed from 3D EBs collected at the different time points (day 8, 10. 11, 14) in culture except for some missing chromosomes at later stages (day 11 to day 14) with no regular pattern. An early study that assessed EBs for their genomic stability using G-banding showed no chromosomal instability [19]. Our data shows that chromosomal aberrations/abnormalities can occur in EBs and karyotyping should be a pre-requisite for studies utilizing EBs. This does not rule out the need for assessing the karyotypes from EBs during propagation. Our data shows that hiPSC derived EB karyotypes change over the day 7 to day 14 period *in vitro* with chromosomal aneuploidy. Such aneuploidies are commonly seen in early human embryo development and have been suggested to be a natural occurrence during meiosis or mitosis [68].

 doi:10.20944/preprints202301.0238.v1

Limitations of Our Study

As this is the first demonstration that applied LSFM and M-FISH karyotyping of iPSC derived EBs, our study has a number of limitations. First of all, it was not possible to continuously image the development of selected EB during few days. In fact, even though during imaging the samples were kept at the correct temperature and humidity and with the right CO2 supply, sterility could not be always guaranteed. This however can be resolved in the future by using a chamber like a microscope incubator from Okolab. Time-lapse imaging of the same EBs at earlier (e.g. days 1-6) and later (day 14 onward) growth would provide information into the complex structure and processes before and after differentiation into different lineages. The inclusion of stage-specific developmental markers would assist in defining the self-organizing capability of iPSC EBs *in vitro*. Furthermore, 3D robust imaging of EB structures, especially from patient-derived iPSCs, will provide disease-specific phenotype and disease modelling. A more extensive analysis by examining many mFISH karyotypes in different iPSC lines would be essential to ascertain the presence of aneuploidies and chromosomal pattern(s) during EB growth. We found difficulties in chromosome sample preparation at later stages of EBs (day 11-14); this requires further protocol optimization.

The assessment of hiPSC derived EBs will have an impact on stem cell research in several areas that include: i) use of different sized EBs for developing standardized protocols allowing efficient and reproducible directed differentiation ii) enhance their use in the study of understanding early embryo development, and iii) assist in the development of iPSCs for disease modeling and clinical applications.

Conclusions

EBs derived from hiPSCs are important intermediates for many biomedical research and clinical applications making their assessment critical. We show that LSFM is a useful technique for investigating the full 3D live volume of iPSC derived EBs allowing information into the morphological changes during their growth. Furthermore, extraction of chromosomes from 3D EBs and whole genome analysis by M-FISH karyotyping is useful for EB development and 3D culture as a whole. Overall, this study shows that cell death in EBs is related to morphological changes and is linked to chromosomal instability at later stages of EB development (day 13 and 14). This study indicates new imaging directions that should be considered in human stem cell research.

Supplementary Materials: The following supporting information can be downloaded at the website of this paper posted on Preprints.org.

Author Contributions: M.Y.: Conceptualization, Methodology, Software, Validation, Formal analysis, Investigation, Data Curation, Writing - Original Draft, Writing - Review & Editing, Visualization, Supervision, Project administration J.S.: Conceptualization, Methodology, Validation, Investigation, Data Curation, Writing - Original Draft, Writing - Review & Editing, Visualization, Project administration S.F.: Software, Validation, Formal analysis, Investigation, Data Curation, Writing - Original Draft, Writing - Review & Editing, Visualization A.C.: Conceptualization, Methodology, Software, Investigation, Resources, Data Curation, Writing - Review & Editing, Project administration, Funding acquisition Archana Bhartiya: Investigation, Data Curation, Writing - Review & Editing A.S.: Software, Validation, Formal analysis, Data Curation, Writing - Original Draft, Writing - Review & Editing, Visualization M.S.: Investigation, Data Curation, Writing - Review & Editing, Project administration Ian K Robinson IK: Conceptualization, Resources, Writing - Review & Editing, Supervision, Project administration, Funding acquisition Stan Botchway: Conceptualization, Methodology, Software, Investigation, Resources, Writing - Review & Editing, Supervision, Project administration, Funding acquisition E.-N.L.: Conceptualization, Methodology, Validation, Resources, Writing - Original Draft, Writing - Review & Editing, Visualization, Supervision, Project administration, Funding acquisition.

Funding: This study was funded by a startup grant by the Centre for Regenerative Medicine and Stem Cell Research at the Aga Khan University. Others include UKRI- Science and Technology Facilities Council (STFC), access to the Central Laser Facility Octopus cluster Application Number 19230009.

Acknowledgments: We thank the Aga Khan University and generous donors for providing support for specialized equipment and the associated data analysis software for the project. The UKRI Science and Technology Facilities Council (STFC), Central Laser Facility Octopus for their continuous support relating the

project and for allowing access to the facility. Finally, we would all like to thank Dr Sally Cowley from the University of Oxford for providing iPSC for the project.

Conflicts of Interest: The authors declare no conflict of interest.

References

1. Takahashi, K., Tanabe, K., Ohnuki, M., Narita, M., Ichisaka, T., Tomoda, K., & Yamanaka, S. (2007). Induction of pluripotent stem cells from adult human fibroblasts by defined factors. *Cell*, *131*(5), 861–872. https://doi.org/10.1016/j.cell.2007.11.019
2. Elitt, M. S., Barbar, L., & Tesar, P. J. (2018). Drug screening for human genetic diseases using iPSC models. *Human Molecular Genetics*, *27*(R2), R89–R98. https://doi.org/10.1093/hmg/ddy186
3. Liu, C., Oikonomopoulos, A., Sayed, N., & Wu, J. C. (2018). Modeling human diseases with induced pluripotent stem cells: From 2D to 3D and beyond. *Development (Cambridge, England)*, *145*(5), dev156166. https://doi.org/10.1242/dev.156166
4. Zhu, Z., & Huangfu, D. (2013). Human pluripotent stem cells: An emerging model in developmental biology. *Development (Cambridge, England)*, *140*(4), 705–717. https://doi.org/10.1242/dev.086165
5. Buchholz, D. E., Hikita, S. T., Rowland, T. J., Friedrich, A. M., Hinman, C. R., Johnson, L. V., & Clegg, D. O. (2009). Derivation of functional retinal pigmented epithelium from induced pluripotent stem cells. *Stem Cells (Dayton, Ohio)*, *27*(10), 2427–2434. https://doi.org/10.1002/stem.189
6. He, Z., Maynard, A., Jain, A., Gerber, T., Petri, R., Lin, H.-C., Santel, M., Ly, K., Dupré, J.-S., Sidow, L., Sanchis Calleja, F., Jansen, S. M. J., Riesenberg, S., Camp, J. G., & Treutlein, B. (2022). Lineage recording in human cerebral organoids. *Nature Methods*, *19*(1), 90–99. https://doi.org/10.1038/s41592-021-01344-8
7. Huch, M., & Koo, B.-K. (2015). Modeling mouse and human development using organoid cultures. *Development (Cambridge, England)*, *142*(18), 3113–3125. https://doi.org/10.1242/dev.118570
8. Simunovic, M., & Brivanlou, A. H. (2017). Embryoids, organoids and gastruloids: New approaches to understanding embryogenesis. *Development (Cambridge, England)*, *144*(6), 976–985. https://doi.org/10.1242/dev.143529
9. Andrews, P. W., Ben-David, U., Benvenisty, N., Coffey, P., Eggan, K., Knowles, B. B., Nagy, A., Pera, M., Reubinoff, B., Rugg-Gunn, P. J., & Stacey, G. N. (2017). Assessing the Safety of Human Pluripotent Stem Cells and Their Derivatives for Clinical Applications. *Stem Cell Reports*, *9*(1), 1–4. https://doi.org/10.1016/j.stemcr.2017.05.029
10. Jo, H. Y., Han, H. W., Jung, I., Ju, J. H., Park, S. J., Moon, S., Geum, D., Kim, H., Park, H. J., Kim, S., Stacey, G. N., Koo, S. K., Park, M. H., & Kim, J. H. (2020). Development of genetic quality tests for good manufacturing practice-compliant induced pluripotent stem cells and their derivatives. *Scientific Reports*, *10*(1). https://doi.org/10.1038/s41598-020-60466-9
11. Kim, J. M., Moon, S.-H., Lee, S. G., Cho, Y. J., Hong, K. S., Lee, J. H., Lee, H. J., & Chung, H.-M. (2011). Assessment of differentiation aspects by the morphological classification of embryoid bodies derived from human embryonic stem cells. *Stem Cells and Development*, *20*(11), 1925–1935. https://doi.org/10.1089/scd.2010.0476
12. Rehakova, D., Souralova, T., & Koutna, I. (2020). Clinical-Grade Human Pluripotent Stem Cells for Cell Therapy: Characterization Strategy. *International Journal of Molecular Sciences*, *21*(7), 2435. https://doi.org/10.3390/ijms21072435
13. Yaffe, M. P., Noggle, S. A., & Solomon, S. L. (2016). Raising the standards of stem cell line quality. *Nature Cell Biology*, *18*(3), 236–237. https://doi.org/10.1038/ncb3313
14. Hwang, Y.-S., Chung, B. G., Ortmann, D., Hattori, N., Moeller, H.-C., & Khademhosseini, A. (2009). Microwell-mediated control of embryoid body size regulates embryonic stem cell fate via differential expression of WNT5a and WNT11. *Proceedings of the National Academy of Sciences of the United States of America*, *106*(40), 16978–16983. https://doi.org/10.1073/pnas.0905550106
15. Messana, J. M., Hwang, N. S., Coburn, J., Elisseeff, J. H., & Zhang, Z. (2008). Size of the embryoid body influences chondrogenesis of mouse embryonic stem cells. *Journal of Tissue Engineering and Regenerative Medicine*, *2*(8), 499–506. https://doi.org/10.1002/term.125
16. Mohr, J. C., Zhang, J., Azarin, S. M., Soerens, A. G., de Pablo, J. J., Thomson, J. A., Lyons, G. E., Palecek, S. P., & Kamp, T. J. (2010). The microwell control of embryoid body size in order to regulate cardiac differentiation of human embryonic stem cells. *Biomaterials*, *31*(7), 1885–1893. https://doi.org/10.1016/j.biomaterials.2009.11.033
17. Conley, B. J., Trounson, A. O., & Mollard, R. (2004). Human embryonic stem cells form embryoid bodies containing visceral endoderm-like derivatives. *Fetal Diagnosis and Therapy*, *19*(3), 218–223. https://doi.org/10.1159/000076701
18. Fridley, K. M., Nair, R., & McDevitt, T. C. (2014b). Differential Expression of Extracellular Matrix and Growth Factors by Embryoid Bodies in Hydrodynamic and Static Cultures. *Tissue Engineering. Part C, Methods*, *20*(12), 931–940. https://doi.org/10.1089/ten.tec.2013.0392

19. Son, M.-Y., Kim, H., Kim, M.-J., & Cho, Y. S. (2011). Physical Passaging of Embryoid Bodies Generated from Human Pluripotent Stem Cells. *PLOS ONE*, *6*(5), e19134. https://doi.org/10.1371/journal.pone.0019134
20. Zhang, Y., Cooke, M., Panjwani, S., Cao, K., Krauth, B., Ho, P.-Y., Medrzycki, M., Berhe, D. T., Pan, C., McDevitt, T. C., & Fan, Y. (2012). Histone H1 Depletion Impairs Embryonic Stem Cell Differentiation. *PLOS Genetics*, *8*(5), e1002691. https://doi.org/10.1371/journal.pgen.1002691
21. Boxman, J., Sagy, N., Achanta, S., Vadigepalli, R., & Nachman, I. (2016). Integrated live imaging and molecular profiling of embryoid bodies reveals a synchronized progression of early differentiation. *Scientific Reports*, *6*(1), 31623. https://doi.org/10.1038/srep31623
22. Méry, A., & Pucéat, M. (2004). Visualisation de la différenciation cellulaire cardiaque par microscopie confocale. *Journal de la Société de Biologie*, *198*(2), 145–151. https://doi.org/10.1051/jbio/2004198020145
23. Adams, M. W., Loftus, A. F., Dunn, S. E., Joens, M. S., & Fitzpatrick, J. A. J. (2015). Light Sheet Fluorescence Microscopy (LSFM). *Current Protocols in Cytometry*, *71*, 12.37.1-12.37.15. https://doi.org/10.1002/0471142956.cy1237s71
24. Huisken, J., Swoger, J., Del Bene, F., Wittbrodt, J., & Stelzer, E. H. K. (2004). Optical sectioning deep inside live embryos by selective plane illumination microscopy. *Science (New York, N.Y.)*, *305*(5686), 1007–1009. https://doi.org/10.1126/science.1100035
25. Pampaloni, F., Ansari, N., & Stelzer, E. H. K. (2013). High-resolution deep imaging of live cellular spheroids with light-sheet-based fluorescence microscopy. *Cell and Tissue Research*, *352*(1), 161–177. https://doi.org/10.1007/s00441-013-1589-7
26. Migliori, B., Datta, M. S., Dupre, C., Apak, M. C., Asano, S., Gao, R., Boyden, E. S., Hermanson, O., Yuste, R., & Tomer, R. (2018). Light sheet theta microscopy for rapid high-resolution imaging of large biological samples. *BMC Biology*, *16*(1), 57. https://doi.org/10.1186/s12915-018-0521-8
27. Stelzer, E. H. K. (2015). Light-sheet fluorescence microscopy for quantitative biology. *Nature Methods*, *12*(1), 23–26. https://doi.org/10.1038/nmeth.3219
28. Ichikawa, T., Nakazato, K., Keller, P. J., Kajiura-Kobayashi, H., Stelzer, E. H. K., Mochizuki, A., & Nonaka, S. (2013). Live Imaging of Whole Mouse Embryos during Gastrulation: Migration Analyses of Epiblast and Mesodermal Cells. *PLOS ONE*, *8*(7), e64506. https://doi.org/10.1371/journal.pone.0064506
29. McDole, K., Guignard, L., Amat, F., Berger, A., Malandain, G., Royer, L. A., Turaga, S. C., Branson, K., & Keller, P. J. (2018). In Toto Imaging and Reconstruction of Post-Implantation Mouse Development at the Single-Cell Level. *Cell*, *175*(3), 859-876.e33. https://doi.org/10.1016/j.cell.2018.09.031
30. Reichmann, J., Eguren, M., Lin, Y., Schneider, I., & Ellenberg, J. (2018). Live imaging of cell division in preimplantation mouse embryos using inverted light-sheet microscopy. *Methods in Cell Biology*, *145*, 279–292. https://doi.org/10.1016/bs.mcb.2018.03.030
31. Strnad, P., Gunther, S., Reichmann, J., Krzic, U., Balazs, B., de Medeiros, G., Norlin, N., Hiiragi, T., Hufnagel, L., & Ellenberg, J. (2016). Inverted light-sheet microscope for imaging mouse pre-implantation development. *Nature Methods*, *13*(2), 139–142. https://doi.org/10.1038/nmeth.3690
32. Ben-David, U., Arad, G., Weissbein, U., Mandefro, B., Maimon, A., Golan-Lev, T., Narwani, K., Clark, A. T., Andrews, P. W., Benvenisty, N., & Carlos Biancotti, J. (2014). Aneuploidy induces profound changes in gene expression, proliferation and tumorigenicity of human pluripotent stem cells. *Nature Communications*, *5*, 4825. https://doi.org/10.1038/ncomms5825
33. Sullivan, S., Stacey, G. N., Akazawa, C., Aoyama, N., Baptista, R., Bedford, P., Bennaceur Griscelli, A., Chandra, A., Elwood, N., Girard, M., Kawamata, S., Hanatani, T., Latsis, T., Lin, S., Ludwig, T. E., Malygina, T., Mack, A., Mountford, J. C., Noggle, S., … Song, J. (2018). Quality control guidelines for clinical-grade human induced pluripotent stem cell lines. *Regenerative Medicine*, *13*(7), 859–866. https://doi.org/10.2217/rme-2018-0095
34. Zambelli, F., Mertens, J., Dziedzicka, D., Sterckx, J., Markouli, C., Keller, A., Tropel, P., Jung, L., Viville, S., Van de Velde, H., Geens, M., Seneca, S., Sermon, K., & Spits, C. (2018). Random Mutagenesis, Clonal Events, and Embryonic or Somatic Origin Determine the mtDNA Variant Type and Load in Human Pluripotent Stem Cells. *Stem Cell Reports*, *11*(1), 102–114. https://doi.org/10.1016/j.stemcr.2018.05.007
35. Amps, K., Andrews, P. W., Anyfantis, G., Armstrong, L., Avery, S., Baharvand, H., Baker, J., Baker, D., Munoz, M. B., Beil, S., Benvenisty, N., Ben-Yosef, D., Biancotti, J.-C., Bosman, A., Brena, R. M., Brison, D., Caisander, G., Camarasa, M. V., Chen, J., … The International Stem Cell Initiative. (2011). Screening ethnically diverse human embryonic stem cells identifies a chromosome 20 minimal amplicon conferring growth advantage. *Nature Biotechnology*, *29*(12), 1132–1144. https://doi.org/10.1038/nbt.2051
36. Lamm, N., Ben-David, U., Golan-Lev, T., Storchová, Z., Benvenisty, N., & Kerem, B. (2016). Genomic Instability in Human Pluripotent Stem Cells Arises from Replicative Stress and Chromosome Condensation Defects. *Cell Stem Cell*, *18*(2), 253–261. https://doi.org/10.1016/j.stem.2015.11.003
37. Moralli, D., Yusuf, M., Mandegar, M. A., Khoja, S., Monaco, Z. L., & Volpi, E. V. (2011). An improved technique for chromosomal analysis of human ES and iPS cells. *Stem Cell Reviews and Reports*, *7*(2), 471–477. https://doi.org/10.1007/s12015-010-9224-4

38. Draper, J. S., Smith, K., Gokhale, P., Moore, H. D., Maltby, E., Johnson, J., Meisner, L., Zwaka, T. P., Thomson, J. A., & Andrews, P. W. (2004). Recurrent gain of chromosomes 17q and 12 in cultured human embryonic stem cells. *Nature Biotechnology*, *22*(1), 53–54. https://doi.org/10.1038/nbt922
39. Maitra, A., Arking, D. E., Shivapurkar, N., Ikeda, M., Stastny, V., Kassauei, K., Sui, G., Cutler, D. J., Liu, Y., Brimble, S. N., Noaksson, K., Hyllner, J., Schulz, T. C., Zeng, X., Freed, W. J., Crook, J., Abraham, S., Colman, A., Sartipy, P., … Chakravarti, A. (2005). Genomic alterations in cultured human embryonic stem cells. *Nature Genetics*, *37*(10), 1099–1103. https://doi.org/10.1038/ng1631
40. Mayshar, Y., Ben-David, U., Lavon, N., Biancotti, J.-C., Yakir, B., Clark, A. T., Plath, K., Lowry, W. E., & Benvenisty, N. (2010). Identification and classification of chromosomal aberrations in human induced pluripotent stem cells. *Cell Stem Cell*, *7*(4), 521–531. https://doi.org/10.1016/j.stem.2010.07.017
41. Taapken, S. M., Nisler, B. S., Newton, M. A., Sampsell-Barron, T. L., Leonhard, K. A., McIntire, E. M., & Montgomery, K. D. (2011). Karotypic abnormalities in human induced pluripotent stem cells and embryonic stem cells. *Nature Biotechnology*, *29*(4), 313–314. https://doi.org/10.1038/nbt.1835
42. Andrews, P. W., Baker, D., Benvinisty, N., Miranda, B., Bruce, K., Brüstle, O., Choi, M., Choi, Y.-M., Crook, J. M., de Sousa, P. A., Dvorak, P., Freund, C., Firpo, M., Furue, M. K., Gokhale, P., Ha, H.-Y., Han, E., Haupt, S., Healy, L., … Zhou, Q. (2015). Points to consider in the development of seed stocks of pluripotent stem cells for clinical applications: International Stem Cell Banking Initiative (ISCBI). *Regenerative Medicine*, *10*(2 Suppl), 1–44. https://doi.org/10.2217/rme.14.93
43. Thompson, O., von Meyenn, F., Hewitt, Z., Alexander, J., Wood, A., Weightman, R., Gregory, S., Krueger, F., Andrews, S., Barbaric, I., Gokhale, P. J., Moore, H. D., Reik, W., Milo, M., Nik-Zainal, S., Yusa, K., & Andrews, P. W. (2020). Low rates of mutation in clinical grade human pluripotent stem cells under different culture conditions. *Nature Communications*, *11*(1), 1528. https://doi.org/10.1038/s41467-020-15271-3
44. Bhaduri, A., Andrews, M. G., Mancia Leon, W., Jung, D., Shin, D., Allen, D., Jung, D., Schmunk, G., Haeussler, M., Salma, J., Pollen, A. A., Nowakowski, T. J., & Kriegstein, A. R. (2020). Cell stress in cortical organoids impairs molecular subtype specification. *Nature*, *578*(7793), 142–148. https://doi.org/10.1038/s41586-020-1962-0
45. Raciti, M., Salma, J., Spulber, S., Gaudenzi, G., Khalajzeyqami, Z., Conti, M., Anderlid, B.-M., Falk, A., Hermanson, O., & Ceccatelli, S. (2019). NRXN1 Deletion and Exposure to Methylmercury Increase Astrocyte Differentiation by Different Notch-Dependent Transcriptional Mechanisms. *Frontiers in Genetics*, *10*, 593. https://doi.org/10.3389/fgene.2019.00593
46. Ahmed, A. R., Candeo, A., D'Abrantes, S., Needham, S. R., Yadav, R. B., Botchway, S. W., & Parker, A. W. (2020). Directly imaging the localisation and photosensitization properties of the pan-mTOR inhibitor, AZD2014, in living cancer cells. *Journal of Photochemistry and Photobiology. B, Biology*, *213*, 112055. https://doi.org/10.1016/j.jphotobiol.2020.112055
47. Sajid, A., Lalani, E.-N., Chen, B., Hashimoto, T., Griffin, D. K., Bhartiya, A., Thompson, G., Robinson, I. K., & Yusuf, M. (2021). Ultra-Structural Imaging Provides 3D Organization of 46 Chromosomes of a Human Lymphocyte Prophase Nucleus. *International Journal of Molecular Sciences*, *22*(11), 5987. https://doi.org/10.3390/ijms22115987
48. Yusuf, M., Leung, K., Morris, K. J., & Volpi, E. V. (2013). Comprehensive cytogenomic profile of the in vitro neuronal model SH-SY5Y. *Neurogenetics*, *14*(1), 63–70. https://doi.org/10.1007/s10048-012-0350-9
49. Bhartiya, A., Robinson, I., Yusuf, M., & Botchway, S. W. (2021). Combining Multicolor FISH with Fluorescence Lifetime Imaging for Chromosomal Identification and Chromosomal Sub Structure Investigation. *Frontiers in Molecular Biosciences*, *8*. https://www.frontiersin.org/article/10.3389/fmolb.2021.631774
50. de Medeiros, G., Balázs, B., & Hufnagel, L. (2016). Light-sheet imaging of mammalian development. *Seminars in Cell & Developmental Biology*, *55*, 148–155. https://doi.org/10.1016/j.semcdb.2015.11.001
51. Adhya, D., Chennell, G., Crowe, J. A., Valencia-Alarcón, E. P., Seyforth, J., Hosny, N. A., Yasvoina, M. V., Forster, R., Baron-Cohen, S., Vernon, A. C., & Srivastava, D. P. (2021). Application of Airy beam light sheet microscopy to examine early neurodevelopmental structures in 3D hiPSC-derived human cortical spheroids. *Molecular Autism*, *12*, 4. https://doi.org/10.1186/s13229-021-00413-1
52. Park, J., Cho, C. H., Parashurama, N., Li, Y., Berthiaume, F., Toner, M., Tilles, A. W., & Yarmush, M. L. (2007). Microfabrication-based modulation of embryonic stem cell differentiation. *Lab on a Chip*, *7*(8), 1018–1028. https://doi.org/10.1039/b704739h
53. Bauwens, C. L., Peerani, R., Niebruegge, S., Woodhouse, K. A., Kumacheva, E., Husain, M., & Zandstra, P. W. (2008). Control of human embryonic stem cell colony and aggregate size heterogeneity influences differentiation trajectories. *Stem Cells (Dayton, Ohio)*, *26*(9), 2300–2310. https://doi.org/10.1634/stemcells.2008-0183
54. Warkus, E. L. L., Yuen, A. A. Y. Q., Lau, C. G. Y., & Marikawa, Y. (2016). Use of In Vitro Morphogenesis of Mouse Embryoid Bodies to Assess Developmental Toxicity of Therapeutic Drugs Contraindicated in Pregnancy. *Toxicological Sciences: An Official Journal of the Society of Toxicology*, *149*(1), 15–30. https://doi.org/10.1093/toxsci/kfv209

55. Pettinato, G., Wen, X., & Zhang, N. (2014). Formation of well-defined embryoid bodies from dissociated human induced pluripotent stem cells using microfabricated cell-repellent microwell arrays. *Scientific Reports*, *4*, 7402. https://doi.org/10.1038/srep07402
56. Itskovitz-Eldor, J., Schuldiner, M., Karsenti, D., Eden, A., Yanuka, O., Amit, M., Soreq, H., & Benvenisty, N. (2000). Differentiation of human embryonic stem cells into embryoid bodies compromising the three embryonic germ layers. *Molecular Medicine (Cambridge, Mass.)*, *6*(2), 88–95
57. Tomov, M. L., Olmsted, Z. T., & Paluh, J. L. (2015). The Human Embryoid Body Cystic Core Exhibits Architectural Complexity Revealed by use of High Throughput Polymer Microarrays. *Macromolecular Bioscience*, *15*(7), 892–900. https://doi.org/10.1002/mabi.201500051
58. Kiene, A. (2012). Formation of Embryoid Bodies from Human Embryonic Stem Cells in Defined Medium. *Biological and Agricultural Engineering Undergraduate Honors Theses*. https://scholarworks.uark.edu/baeguht/20
59. Bader, A., Gruss, A., Höllrigl, A., Al-Dubai, H., Capetanaki, Y., & Weitzer, G. (2001). Paracrine promotion of cardiomyogenesis in embryoid bodies by LIF modulated endoderm. *Differentiation; Research in Biological Diversity*, *68*(1), 31–43. https://doi.org/10.1046/j.1432-0436.2001.068001031.x
60. Fuchs, C., Scheinast, M., Pasteiner, W., Lagger, S., Hofner, M., Hoellrigl, A., Schultheis, M., & Weitzer, G. (2012). Self-organization phenomena in embryonic stem cell-derived embryoid bodies: Axis formation and breaking of symmetry during cardiomyogenesis. *Cells, Tissues, Organs*, *195*(5), 377–391. https://doi.org/10.1159/000328712
61. Weitzer, G. (2006). Embryonic stem cell-derived embryoid bodies: An in vitro model of eutherian pregastrulation development and early gastrulation. *Handbook of Experimental Pharmacology*, *174*, 21–51
62. Carpenedo, R. L., Sargent, C. Y., & McDevitt, T. C. (2007). Rotary suspension culture enhances the efficiency, yield, and homogeneity of embryoid body differentiation. *Stem Cells (Dayton, Ohio)*, *25*(9), 2224–2234. https://doi.org/10.1634/stemcells.2006-0523
63. Gothard, D., Roberts, S. J., Shakesheff, K. M., & Buttery, L. D. (2009). Controlled embryoid body formation via surface modification and avidin-biotin cross-linking. *Cytotechnology*, *61*(3), 135–144. https://doi.org/10.1007/s10616-010-9255-3
64. Van Winkle, A. P., Gates, I. D., & Kallos, M. S. (2012). Mass transfer limitations in embryoid bodies during human embryonic stem cell differentiation. *Cells, Tissues, Organs*, *196*(1), 34–47. https://doi.org/10.1159/000330691
65. Lancaster, M. A. (2018). Brain organoids get vascularized. *Nature Biotechnology*, *36*(5), 407–408. https://doi.org/10.1038/nbt.4133
66. Simon, M. C., & Keith, B. (2008). The role of oxygen availability in embryonic development and stem cell function. *Nature Reviews. Molecular Cell Biology*, *9*(4), 285–296. https://doi.org/10.1038/nrm2354
67. Popp, B., Krumbiegel, M., Grosch, J., Sommer, A., Uebe, S., Kohl, Z., Plötz, S., Farrell, M., Trautmann, U., Kraus, C., Ekici, A. B., Asadollahi, R., Regensburger, M., Günther, K., Rauch, A., Edenhofer, F., Winkler, J., Winner, B., & Reis, A. (2018). Need for high-resolution Genetic Analysis in iPSC: Results and Lessons from the ForIPS Consortium. *Scientific Reports*, *8*(1), 17201. https://doi.org/10.1038/s41598-018-35506-0
68. Lee, A., & Kiessling, A. A. (2017). Early human embryos are naturally aneuploidy-Can that be corrected? *Journal of Assisted Reproduction and Genetics*, *34*(1), 15–21. https://doi.org/10.1007/s10815-016-0845-7.